Numerical Magnetohydrodynamics and Extended MHD for Magnetic Confinement

Carl R. Sovinec
University of Wisconsin-Madison

43rd IEEE International Conference on Plasma Science
Mini-course on Plasma Simulation
June 24, 2016 Banff, Alberta, Canada

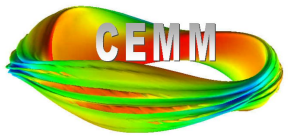

Introduction: Magnetic confinement systems are rich in macroscopic dynamics, and …

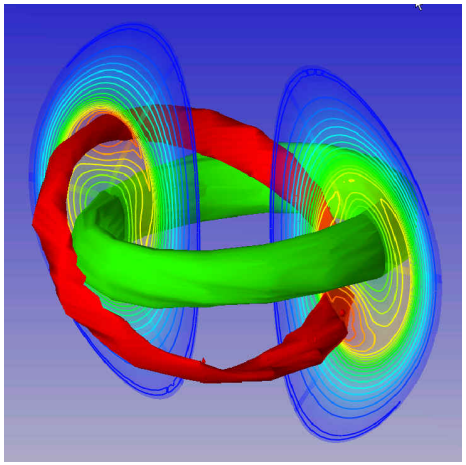

Simulation of internal kink in NSTX by W. Park, PPPL.

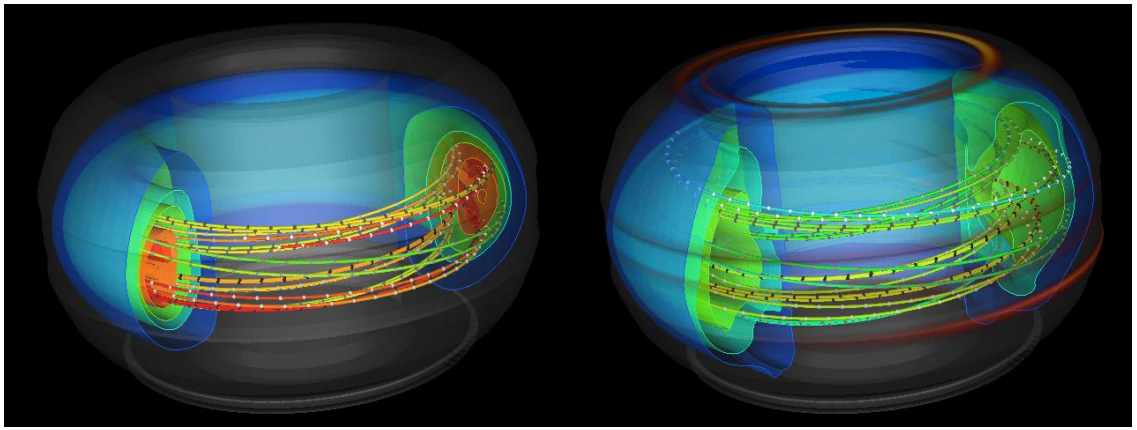

High-pressure disruption simulation by S. Kruger and A. Sanderson [Phys. Plasmas **12**, 56113].

- Tokamak sawteeth
  - Magnetic reconnection
  - Energetic-particle effects
- Tokamak disruption
  - Multi-physics effects in different forms of disruption
  - Mitigation systems

… numerical simulation of macroscopic dynamics provides important information.

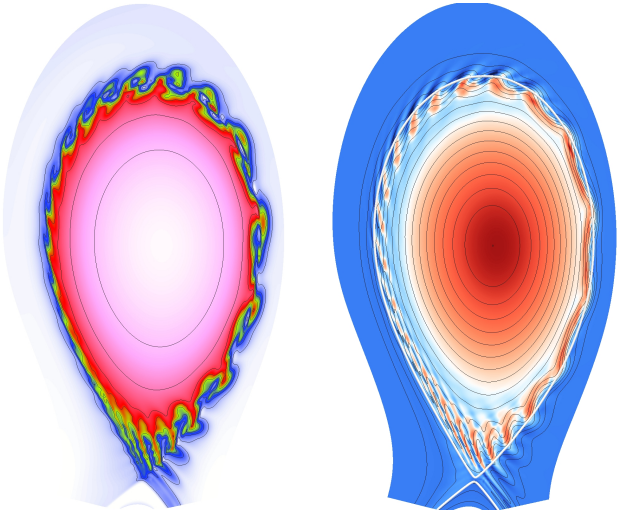

Particle and current density from an ELM simulation by G. Huysmans [PPCF **51**, 124012].

- Edge-localized modes (ELMs)
  - Mode coupling
  - Resonant perturbation effects
- Magnetic relaxation
  - Magnetic island evolution
  - Dynamo effects in RFPs and spheromaks
  - Non-inductive current drive

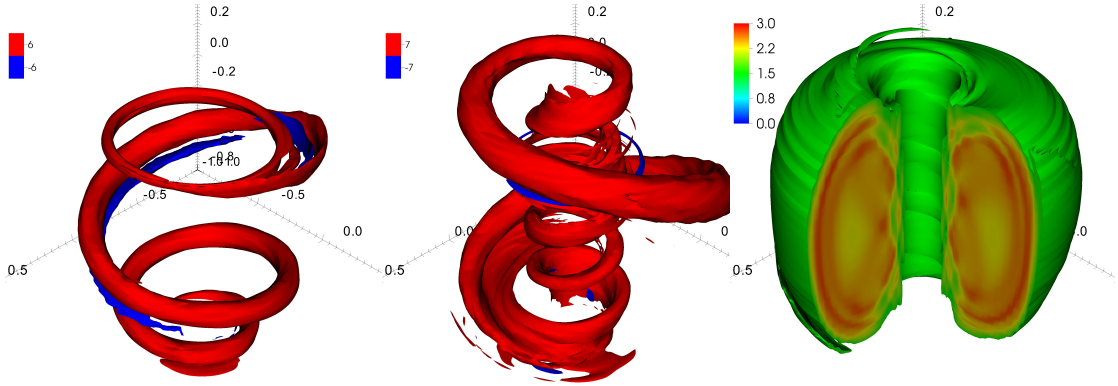

Simulation of Pegasus startup by J. O'Bryan [PPCF **56**, 064005].

Outline

- Introduction
- Background
  - Physical parameters
  - Confinement and sources of free energy
  - Resonances
- Pertinent examples
- Models for macroscopic dynamics
  - Primitive-variable systems
  - Reduced systems
- Numerical methods
  - Time-advance
  - Spatial representation
- Parallel computing
- Open challenges and outlook

Background: Physical properties of confined plasma influence the selection of numerical methods.

- Separation of scales (medium sized tokamak)
  - Global Alfvén propagation time τ_A ~ 0.3 μs
  - Particle collision times τ_e ~ 0.2 ms, τ_i ~ 15 ms
  - Global resistive diffusion time τ_r ~ 1-10 s (S = τ_r/τ_A)
  - Sound gyroradius $\rho_s = (m_i k_B T_e/q_i^2 B^2)^{1/2}$ ~ 5 mm
  - Minor radius a ~ 0.5 m
- Extreme anisotropy relative to **B**(**x**,t)
  - Effective thermal diffusivity ratio $\chi_{\|}/\chi_{\perp} >> 10^6$
  - Also extreme anisotropy for viscous diffusivities
- Nonlinear conditions remain close to force-balance
  - No shock propagation
  - Distinct force-density contributions nearly cancel

Toroidal magnetic confinement has two primary sources of free energy for MHD.

- Toroidal geometry avoids end losses.
- **B** must twist to prevent net outward drifts.
- Field-lines trace-out flux surfaces.

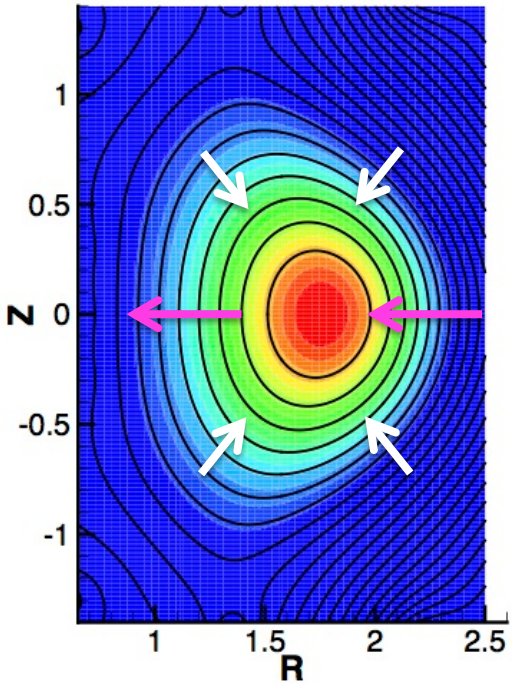

Cross section of plasma pressure contours (color) and magnetic flux (black lines). $\boldsymbol{\kappa}$ from $\mathbf{B}_{pol}$ (white) and from B_ϕ (magenta).

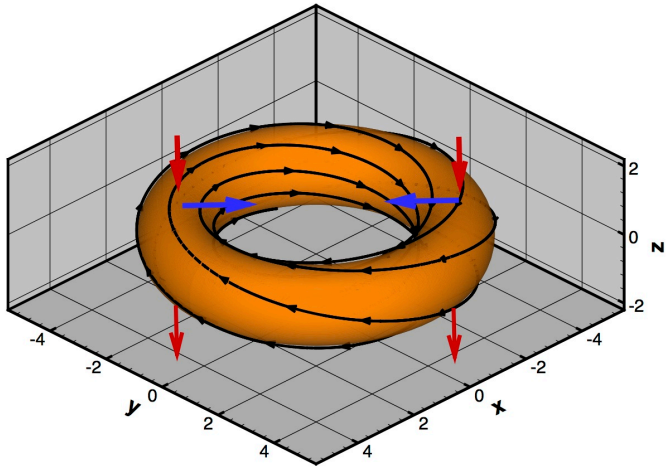

Illustration showing **B** (black), ∇B vectors (blue) and resulting ion particle drifts (red).

- #1) The alignment of curvature $\boldsymbol{\kappa} = \hat{\mathbf{b}} \cdot \nabla \hat{\mathbf{b}}$ with ∇P leads to free energy; the perturbed ideal-MHD energy contribution is

$$-\int_{R_{pl}} \left(\vec{\xi}_\perp \cdot \nabla P\right)\left(\vec{\xi}_\perp^{\,*} \cdot \boldsymbol{\kappa}\right) dVol \;\sim\; \mathbf{F} \cdot \Delta \mathbf{s}$$

There are two primary sources of free energy (cont).

- In axisymmetric systems, twist is provided by charge current running through the plasma.
- Except in FRCs, current density is largely parallel to **B**.

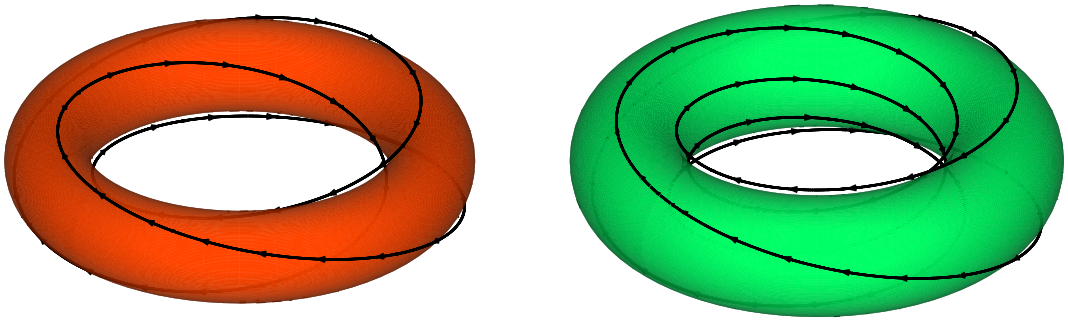

Two surfaces of the same configuration showing 3/2 (left) and 5/2 (right) twist, i.e. safety factor (q).

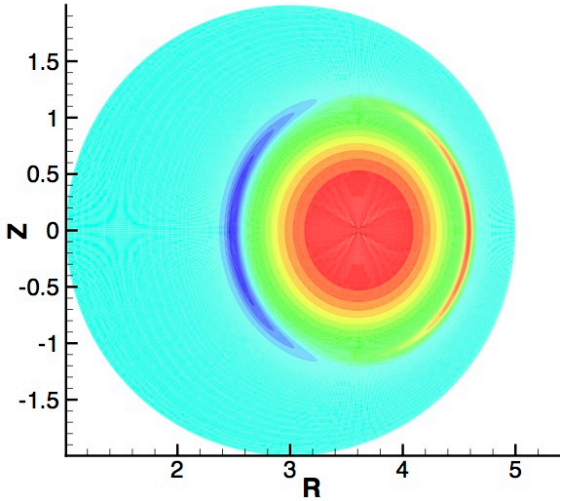

Contour plot of λ for the same configuration shows significant spatial variation.

- #2) Spatial variation of the "parallel" current density, $\lambda = J_{||}/B$, also contributes free energy:

$$-\int_{R_{pl}} \lambda\left(\vec{\xi}_{\perp}^{*}\times\mathbf{B}\right)\cdot\nabla\times\left(\vec{\xi}_{\perp}\times\mathbf{B}\right)dVol \sim I\,V\,\Delta t$$

Resonance for helical shear-Alfvén waves occurs along toroidal surfaces.

- Restoring force density from bending is weak where wavefronts align with $\mathbf{B}_0$, hence susceptibility to instability.
- Resonant instability in sheared field leads to spatial localization.

Background magnetic field is sheared.

Rational-winding wavefronts align with $\mathbf{B_0}$ along the resonant surface ($\mathbf{k}\cdot\mathbf{B_0} = 0$).

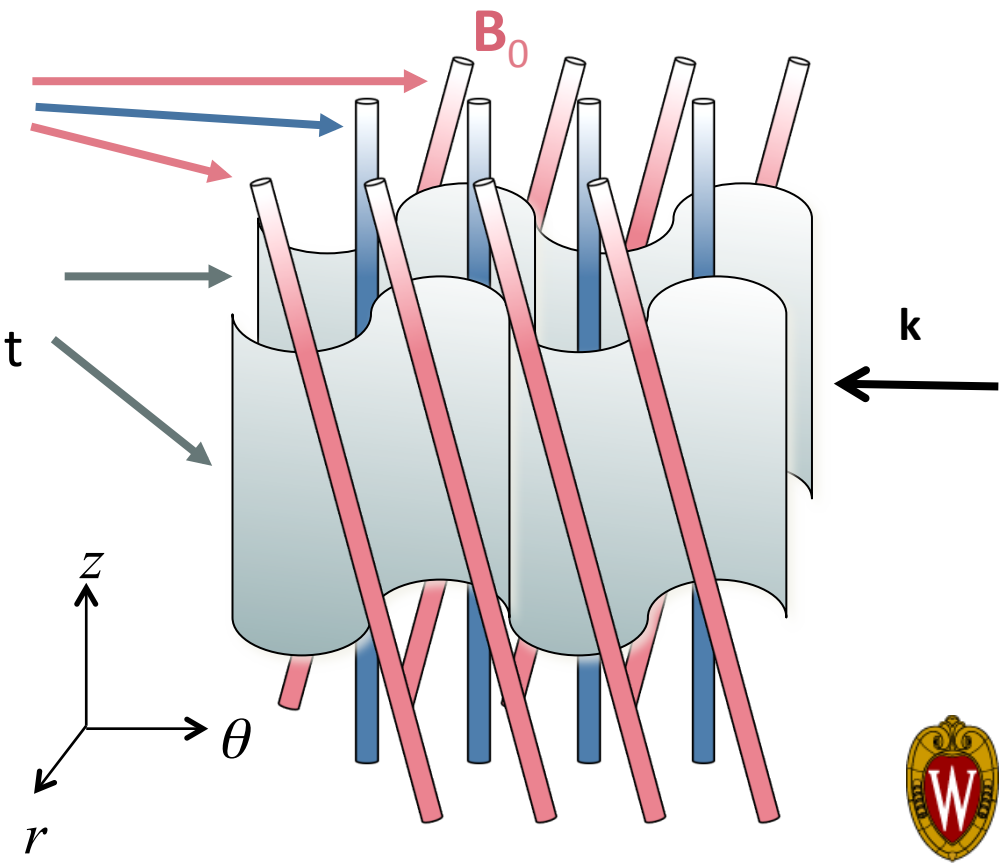

Pertinent examples: Non-ideal effects lead to changes in magnetic topology.

- Resistive or other non-ideal effects allow instabilities when free energy is insufficient for ideal-MHD instability.
- Magnetic reconnection (from $\nabla\lambda$ energy) at resonances leads to helical islands.
- Island overlap produces regions of stochastic magnetic field.

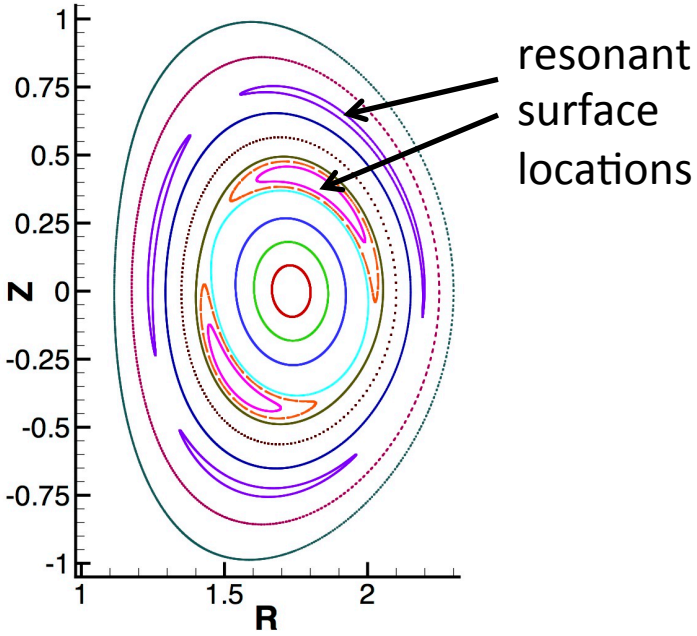

Cross-sections of islands are embedded among toroidal flux surfaces.

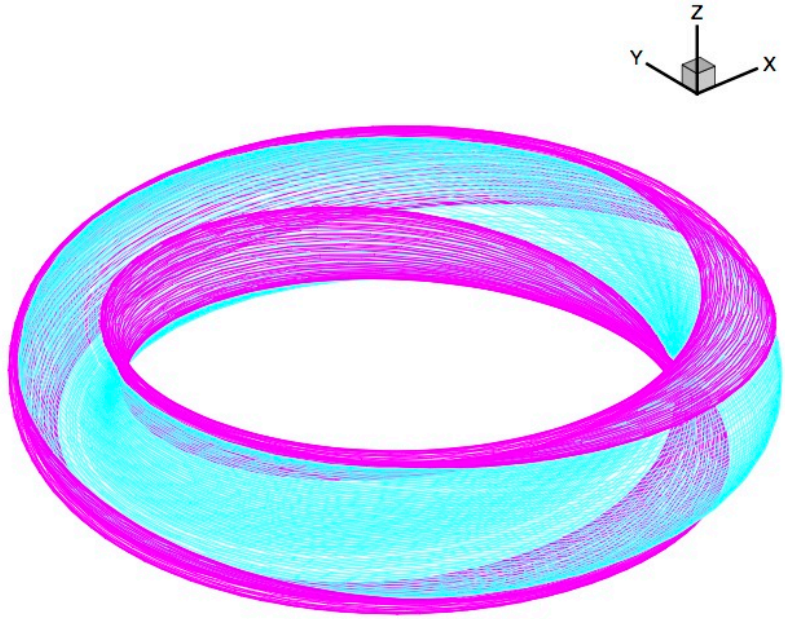

Non-overlapping islands are distinct regions but enhance energy transport.

Interchange can localize on the outboard side of a torus, leading to ballooning instability.

- Like other interchange activity, dynamics are largely perpendicular to **B**.
- Instability tends to arise over a broad range of toroidal wavenumbers; two-fluid and kinetic effects can be important.
- Ballooning can cause disruption or edge-localized modes (ELMs).

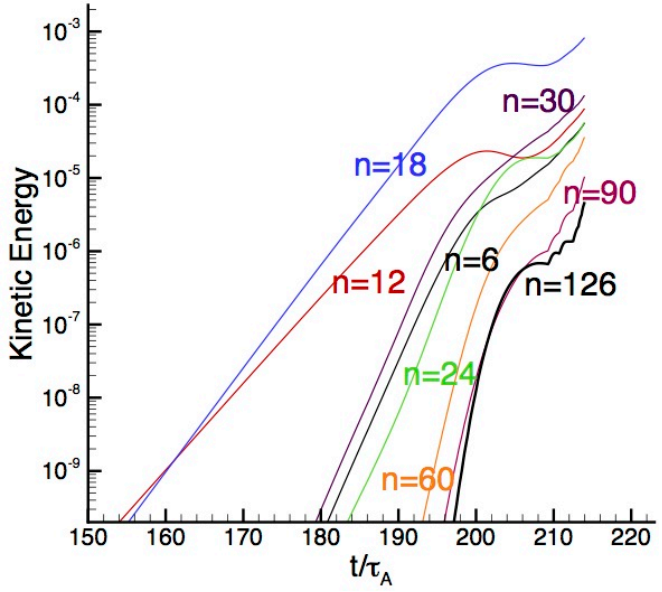

A computation run with limited periodicity has 2 linearly unstable wave-numbers.

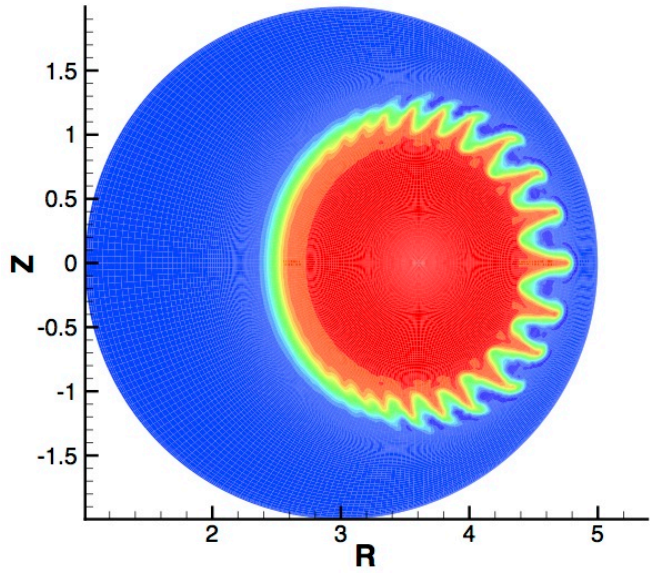

Nonlinear evolution produces helical fingers of density and energy.

Models: We distinguish primitive-field and potential-field systems of equations.

- Primitive-field models describe the evolution of low-order moments of particle distributions and low-frequency electromagnetics.*

$$\frac{\partial n}{\partial t} + \nabla \cdot \left(n\mathbf{V} \right) = 0$$ particle continuity

$$mn\left(\frac{\partial}{\partial t} + \mathbf{V} \cdot \nabla \right) \mathbf{V} = \mathbf{J} \times \mathbf{B} - \nabla p - \nabla \cdot \underline{\Pi}$$ momentum density

$$\frac{\partial \mathbf{B}}{\partial t} = -\nabla \times \mathbf{E}$$ Faraday's law

$$\mu_0 \mathbf{J} = \nabla \times \mathbf{B}$$ Ampere's law

$$\nabla \cdot \mathbf{B} = 0$$ divergence constraint

- The model also needs closure information and a generalized Ohm's law for **E**.

*See [Kimura and Morrison, PoP **21**, 082101] for energy considerations.

The remaining relations select the level of physics fidelity.

- The generalized Ohm's law extracts a low-frequency relation for **E** from electron momentum-density evolution.

$$\mathbf{E} = -\mathbf{V}\times\mathbf{B} + \eta\mathbf{J} + \frac{1}{ne}\left(\mathbf{J}\times\mathbf{B} - \nabla p_e\right) + \frac{1}{\varepsilon_0\omega_{pe}^2}\left[\frac{\partial}{\partial t}\mathbf{J} + \nabla\cdot\left(\mathbf{JV}+\mathbf{VJ}\right)\right]$$

ideal MHD; resistive **E**; Hall and e^- pressure; e^- inertia

- Stress may be a combination of effects.

$$\underline{\mathbf{W}} \equiv \nabla\mathbf{V} + \nabla\mathbf{V}^{\mathrm{T}} - \frac{2}{3}\underline{\mathbf{I}}\nabla\cdot\mathbf{V}$$

$$\underline{\Pi}_{\mathrm{gv}} = \frac{m_{\mathrm{i}}p_{\mathrm{i}}}{4eB}\left[\hat{\mathbf{b}}\times\underline{\mathbf{W}}\cdot\left(\underline{\mathbf{I}}+3\hat{\mathbf{b}}\hat{\mathbf{b}}\right) - \left(\underline{\mathbf{I}}+3\hat{\mathbf{b}}\hat{\mathbf{b}}\right)\cdot\underline{\mathbf{W}}\times\hat{\mathbf{b}}\right]$$ gyroviscosity

$$\underline{\Pi}_{\parallel} = \frac{p_i\tau_i}{2}\left(\hat{\mathbf{b}}\cdot\underline{\mathbf{W}}\cdot\hat{\mathbf{b}}\right)\left(\underline{\mathbf{I}}-3\hat{\mathbf{b}}\hat{\mathbf{b}}\right)$$ parallel

$$\underline{\Pi}_{\perp} \sim -\frac{3p_i m_i^2}{10e^2B^2\tau_i}\underline{\mathbf{W}} \Rightarrow -nm_i\nu_{iso}\,\underline{\mathbf{W}} \text{ or } -nm_i\nu_{kin}\,\nabla\mathbf{V}$$ perpendicular

The closure relation for pressure(s) is selected for the dynamics of interest.

- At sufficiently low plasma-β (= $\mu_0 p/B^2$), pressure can be dropped.

  $$p = 0$$

- If compressive waves are faster than all dynamics of interest, flow may be incompressible.

  $$\nabla \cdot \mathbf{V} = 0$$

- An adiabatic relation describes fast perpendicular dynamics.

  $$\frac{\partial}{\partial t} p + \mathbf{V} \cdot \nabla p = -\Gamma p \nabla \cdot \mathbf{V}$$

- Otherwise, an energy equation with heat-flux-density closure is used.

  $$\frac{n_s}{\Gamma - 1}\left(\frac{\partial}{\partial t} T_s + \mathbf{V}_s \cdot \nabla T_s\right) = -n_s T_s \nabla \cdot \mathbf{V}_s - \nabla \cdot \mathbf{q}_s + Q_s \qquad s = i, e$$

  $$\mathbf{q}_s = \underbrace{-n_s\left(\chi_{\parallel} - \chi_{\perp}\right)\hat{\mathbf{b}}\hat{\mathbf{b}} \cdot \nabla T_s - n_s \chi_{\perp} \nabla T_s}_{\text{anisotropic conduction}} + \underbrace{\frac{5 n_s T_s}{2 q_s B}\hat{\mathbf{b}} \times \nabla T_s}_{\text{magnetization } \mathbf{q}}$$

Closure information can be obtained from kinetic computations.

- PIC computations have been used for a hot-ion component [Park, et al., PFB **4**, 2033; Kim, PoP **15**, 072507].
  - Low n_{hot} and $mn_{hot}\mathbf{V}_{hot}$ are assumed.
  - Coupling to $\mathbf{V}_{COM}$ evolution is through hot-particle stress or current.
  - Applications include energetic-particle modes, sawteeth, and tearing.
- Eulerian δf drift-kinetics can be used to close majority-species equations.
  - Consistent kinetic model has been derived [Ramos, PoP **15**, 082106].
  - The kinetic computations have been solved and verified in the framework of an extended-MHD code [Held, et al., PoP **22** 032511].

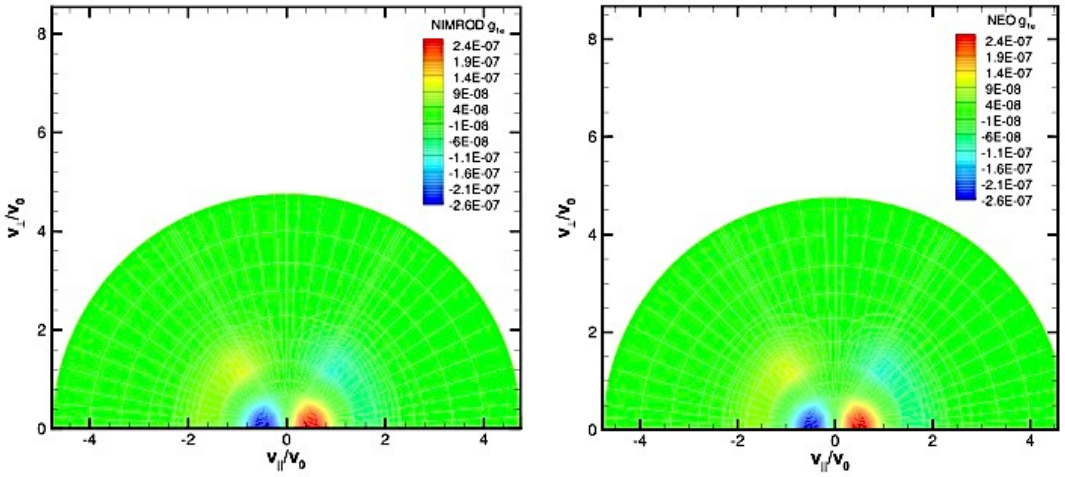

Verification of the NIMROD implementation with NEO includes e^- distribution and bootstrap current [Held].

Potential formulations separate physical effects among the variables, themselves.

- The basic version is reduced MHD [Strauss, PoF **18**, 134], which orders tokamak fields by $\varepsilon = a/R$.
  - Twist of $O(1)$ implies $B_{pol} \sim \varepsilon B_\phi$ and $\beta \sim \varepsilon^2$.
  - Dynamics with $k_{||}/k_\perp << 1$ have $\mathbf{V}_\perp = \hat{\mathbf{b}}_0 \times \nabla\varphi$ at lowest order, where φ is the electrostatic potential.
  - The lowest-order perturbed field is $\mathbf{B}_1 = \nabla\psi \times \mathbf{B}_0$.
- A reduced resistive-MHD system is [Hazeltine and Meiss (1992)]:

$$\rho_0 \frac{\partial}{\partial t}\nabla_f^2\varphi = -\frac{B_0^2}{\mu_0}\nabla_{||}\nabla_f^2\psi + 2\hat{\mathbf{b}}_0 \times \boldsymbol{\kappa}\cdot\nabla_f p \qquad \text{parallel vorticity evolution}$$

$$\frac{\partial}{\partial t}\psi = -\frac{1}{B_0}\nabla_{||}\left(B_0\varphi\right) + \frac{\eta}{\mu_0}\nabla_f^2\psi \qquad \text{parallel Ohm's law}$$

$$\frac{\partial}{\partial t}p = \hat{\mathbf{b}}_0 \times \nabla p_0 \cdot \nabla_f\varphi \qquad \text{pressure advection}$$

- For $\varepsilon << 1$, || is the toroidal direction and ∇_f is the poloidal gradient.

The choice of model has ramifications for numerical computation.

- Potential-based systems [e.g. Breslau, Ferraro, Jardin, PoP **16**, 092503]
  - Numerical operations on scalars are relatively straightforward.
  - Potentials can avoid numerical coupling of physical effects.
  - Higher-order differentiation or use of auxiliary variables is required.
  - Non-reduced equations are more complicated than the vector moment relations.
- Primitive-field systems [e.g. Sovinec, et al., JCP **195**, 355]
  - Vector calculus is not trivial, numerically.
  - Separating distinct physical effects relies on numerics.
  - Equations are directly from moment relations.
  - Representations can use lower-order continuity.

Numerical methods (part 1): Some form of implicit computation is needed.

- Nonlinear evolution occurs over long time-scales.
  - Virulent ELMs occur over 10s of τ_A.
  - Resistive island evolution and relaxation occur over tenths of τ_r.
- Wave-CFL condition restricts explicit computation.
  - Resolving resonances requires $\Delta x < \rho_s$.
  - $\Delta x < R/1000$ implies 1000s of steps for each τ_A of an explicit simulation.
- A number of implicit methods have been applied to MHD for magnetic confinement.
  - Many fall into the class of methods now labeled "IMEX" in applied math.

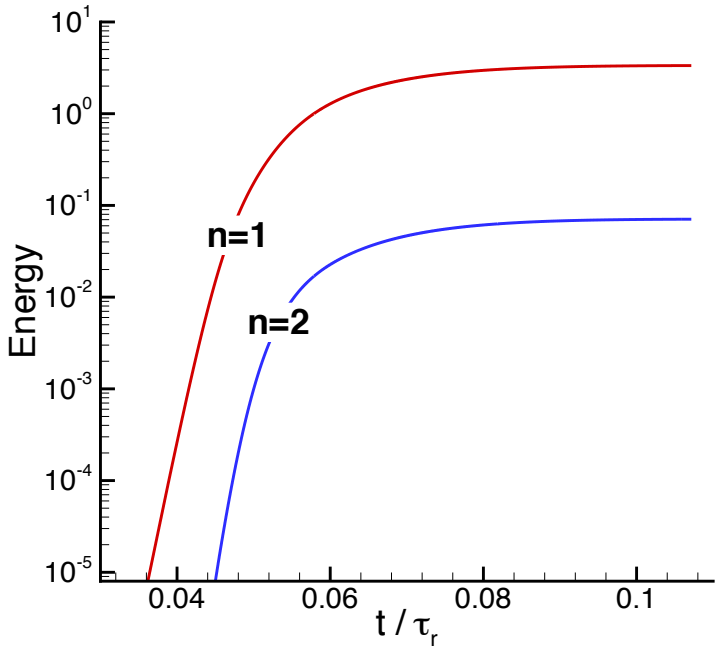

Development of magnetic island shown earlier occurs over ~ 10^5 τ_A.

A simple example illustrates practical alternatives.

- Take the cylindrical-geometry approximation with uniform $\mathbf{B}_0 = B_0\hat{\mathbf{z}}$ and vanishingly small β.
  - The ∇_f^2 operator can be inverted.
  - In the simplified, reduced system with $\eta = 0$, small perturbations of the form $f(r)\exp\left[im\theta + ikz\right]$ evolve according to

$$\frac{\partial}{\partial t}\varphi_{m,k} = -v_A^2\nabla_{\parallel}\psi_{m,k} \rightarrow -ikv_A^2\psi_{m,k} \qquad v_A^2 = B_0^2/\mu_0\rho_0$$

$$\frac{\partial}{\partial t}\psi_{m,k} = -\nabla_{\parallel}\varphi_{m,k} \rightarrow -ik\varphi_{m,k}$$

Explicit methods are limited by the *CFL* condition.

- Apply an explicit leapfrog time-advance ($t^n = n\Delta t$) to the simplified shear-wave system:

$$\varphi_{m,k}^{n+1} - \varphi_{m,k}^{n} = -ik\Delta t\, v_A^2 \psi_{m,k}^{n}$$
$$\psi_{m,k}^{n+1} - \psi_{m,k}^{n} = -ik\Delta t\, \varphi_{m,k}^{n+1}$$

- Taking ξ as the eigenvalue of the time-step operation,

$$(\xi - 1)\varphi_{m,k} = -ik\Delta t\, v_A^2 \psi_{m,k}$$
$$(\xi - 1)\psi_{m,k} = -ik\Delta t\, \xi\, \varphi_{m,k}$$

- Solutions of the characteristic equation, $(\xi - 1)^2 + k^2 v_A^2 \Delta t^2 \xi = 0$, have

$$|\xi| > 1,\ \Delta t > \frac{2}{k v_A} \quad \rightarrow \quad \text{unphysical growth (linear numerical instability)}$$

$$|\xi| = 1,\ \Delta t \le \frac{2}{k v_A} \quad \rightarrow \quad \text{stable oscillation}$$

Implicit methods allow numerical stability at large time-step values.

- A flexible method evaluates the drive terms at f into the step ($0 \le f \le 1$):

$$\varphi_{m,k}^{n+1} - \varphi_{m,k}^{n} = -ik\Delta t\, v_A^2 \left[f\psi_{m,k}^{n+1} + (1-f)\psi_{m,k}^{n} \right]$$

$$\psi_{m,k}^{n+1} - \psi_{m,k}^{n} = -ik\Delta t \left[f\varphi_{m,k}^{n+1} + (1-f)\varphi_{m,k}^{n} \right]$$

- Taylor-expanding the analytical solution about $t^n + \frac{1}{2}\Delta t$ and inserting into the approximation, to $O(\Delta t^2)$,

$$\left(\frac{\partial}{\partial t} + \frac{\Delta t^2}{24}\frac{\partial^3}{\partial t^3} \right) \begin{pmatrix} \varphi_{m,k} \\ \psi_{m,k} \end{pmatrix} = -ik \left[1 + \Delta t \left(f - \frac{1}{2} \right) \frac{\partial}{\partial t} + \frac{\Delta t^2}{8}\frac{\partial^2}{\partial t^2} \right] \begin{pmatrix} v_A^2 \psi_{m,k} \\ \varphi_{m,k} \end{pmatrix}$$

- Keeping the lowest-order terms, the differential approximation [Shokin (1983)] can be expressed as

$$\frac{\partial}{\partial t} \begin{pmatrix} \varphi_{m,k} \\ \psi_{m,k} \end{pmatrix} = -ik \begin{pmatrix} v_A^2 \psi_{m,k} \\ \varphi_{m,k} \end{pmatrix} - \Delta t \left(f - \frac{1}{2} \right) k^2 v_A^2 \begin{pmatrix} \varphi_{m,k} \\ \psi_{m,k} \end{pmatrix}$$

★ k^2 represents $-\nabla_{\|}^2$, so the last term adds numerical damping for $f > \frac{1}{2}$.

Researchers have used alternatives to full implicit methods.

- Implicit computations solve algebraic systems at each step.
  - Coefficients of the spatial expansion are coupled at the new time.
  - Full implicit methods solve nonlinear algebraic systems.
  - System size, condition number, sparsity, and linear vs. nonlinear affect computational cost per step.
- The "quasi-implicit" method uses the large-R/a ordering and treats only poloidal compression implicitly [Park and Monticello, NF **30**, 285].
  - The potential formulation separates poloidal compression to keep algebraic systems small and linear (original M3D).
  - Shear waves (explicit) diminish computational gains at moderate R/a.
- "Semi-implicit" methods add numerical dispersion to stabilize the advance [Schnack, et al., JCP **70**, 330] (DEBS, original XTOR, NIMROD).

The semi-implicit leapfrog is compatible with primitive-field representations.

- Add a positive spatial differential operator $-\Delta t^2 \underline{\mathbf{L}}$ to staggered leapfrog for linear ideal-MHD--dropping continuity and pressure for clarity:

$$\left(\rho_0 - \Delta t^2 \underline{\mathbf{L}}\right)\left(\mathbf{V}^{n+1} - \mathbf{V}^n\right) = \Delta t\left(\mathbf{J}^{n+1/2} \times \mathbf{B}_0 + \mathbf{J}_0 \times \mathbf{B}^{n+1/2}\right)$$

$$\mathbf{B}^{n+1/2} - \mathbf{B}^{n-1/2} = \Delta t \nabla \times \left(\mathbf{V}^n \times \mathbf{B}_0\right)$$

- The differential approximation for the original initial conditions [Caramana, JCP **96**, 484] and with synchronization [Sovinec & King, JCP **229**, 5803] is

$$\left(\rho_0 - \Delta t^2 \mathbf{L}\right)\frac{\partial}{\partial t}\mathbf{V}\bigg|_{t^{n+1/2}} = \frac{1}{\mu_0}\nabla \times \left(\mathbf{B} + \frac{\Delta t}{2}\frac{\partial}{\partial t}\mathbf{B}\right)\bigg|_{t^n} \times \mathbf{B}_0 + \mathbf{J}_0 \times \left(\mathbf{B} + \frac{\Delta t}{2}\frac{\partial}{\partial t}\mathbf{B}\right)\bigg|_{t^n}$$

$$\frac{\partial}{\partial t}\mathbf{B}\bigg|_{t^n} = \nabla \times \left[\left(\mathbf{V} - \frac{\Delta t}{2}\frac{\partial}{\partial t}\mathbf{V}\right)\bigg|_{t^{n+1/2}} \times \mathbf{B}_0\right]$$

Manipulating the differential approximation shows the numerical properties of the semi-implicit method.

- The equations can be combined to produce the second-order

$$\left(\rho_0 + \frac{\Delta t^2}{4}\underline{\mathbf{F}}_0 - \Delta t^2 \underline{\mathbf{L}}\right)\frac{\partial^2}{\partial t^2}\mathbf{V} = \underline{\mathbf{F}}_0(\mathbf{V})$$

  where $\underline{\mathbf{F}}_0$ is the linear ideal-MHD force operator.

- Modes of the linear ideal-MHD system satisfy $\underline{\mathbf{F}}_0(\xi) = -\rho_0\omega^2\xi$.
- In the absence of the semi-implicit operator, the system is ill-posed, i.e. numerically unstable if $\Delta t^2 > 4/\omega^2$ for the largest ω^2.
- $\underline{\mathbf{L}}$ can be selected for accuracy and computational practicality:

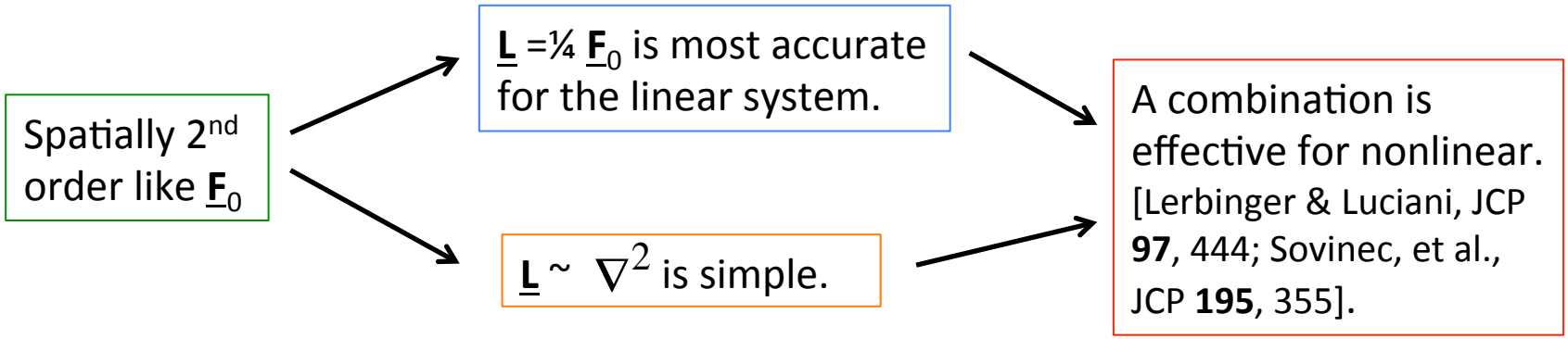

Implicitly balanced methods avoid truncation errors from separating ("splitting") physics.

- Quasi- and semi-implicit methods use various levels of splitting.
- Balanced methods determine all fields at the new time-level, simultaneously.
  - This improves multi-scale convergence [Knoll, et al. JCP **185**, 583].
  - A simple analysis for $du/dt = \gamma_0 u$ with Crank-Nicolson (implicit f = ½) is

$$\gamma_{CN} = \frac{\ln(\xi_{\mathrm{CN}})}{\Delta t} = \frac{1}{\Delta t}\ln\left(\frac{2+\gamma_0\Delta t}{2-\gamma_0\Delta t}\right)$$

- Modern Krylov-space algebraic solvers + Newton's method facilitate balanced nonlinear MHD computation [Chacón, PoP **15**, 056102].
- Avoiding numerical dissipation is important for simulating high temperatures.

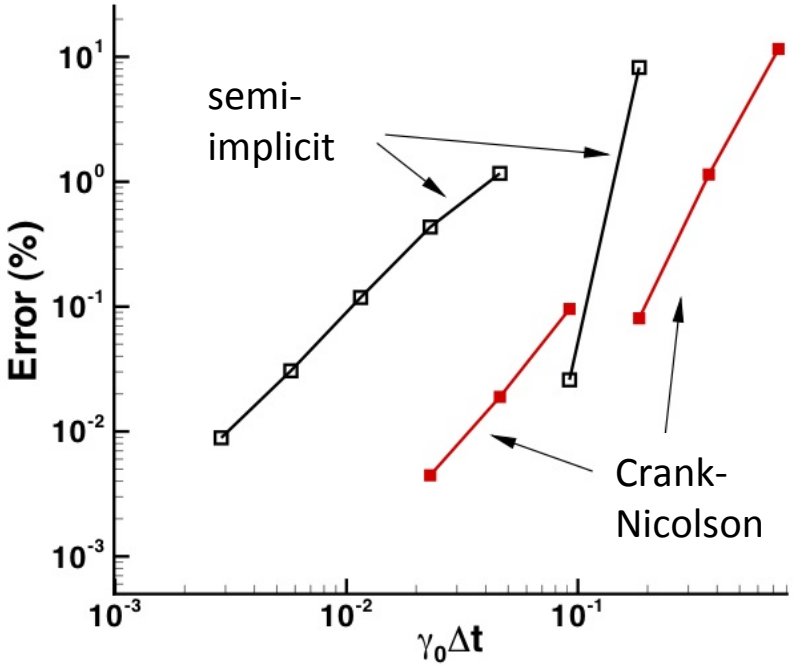

Tearing-mode comparison of C-N and SI [JCP **229**, 5803] for two-fluid.

Numerical methods (part 2): There are several considerations for spatial representations.

- Accurate representation of $\hat{\mathbf{b}}\cdot\nabla$ is important for force equilibration.
- Anisotropic transport also depends on the evolving $\hat{\mathbf{b}}\cdot\nabla$.

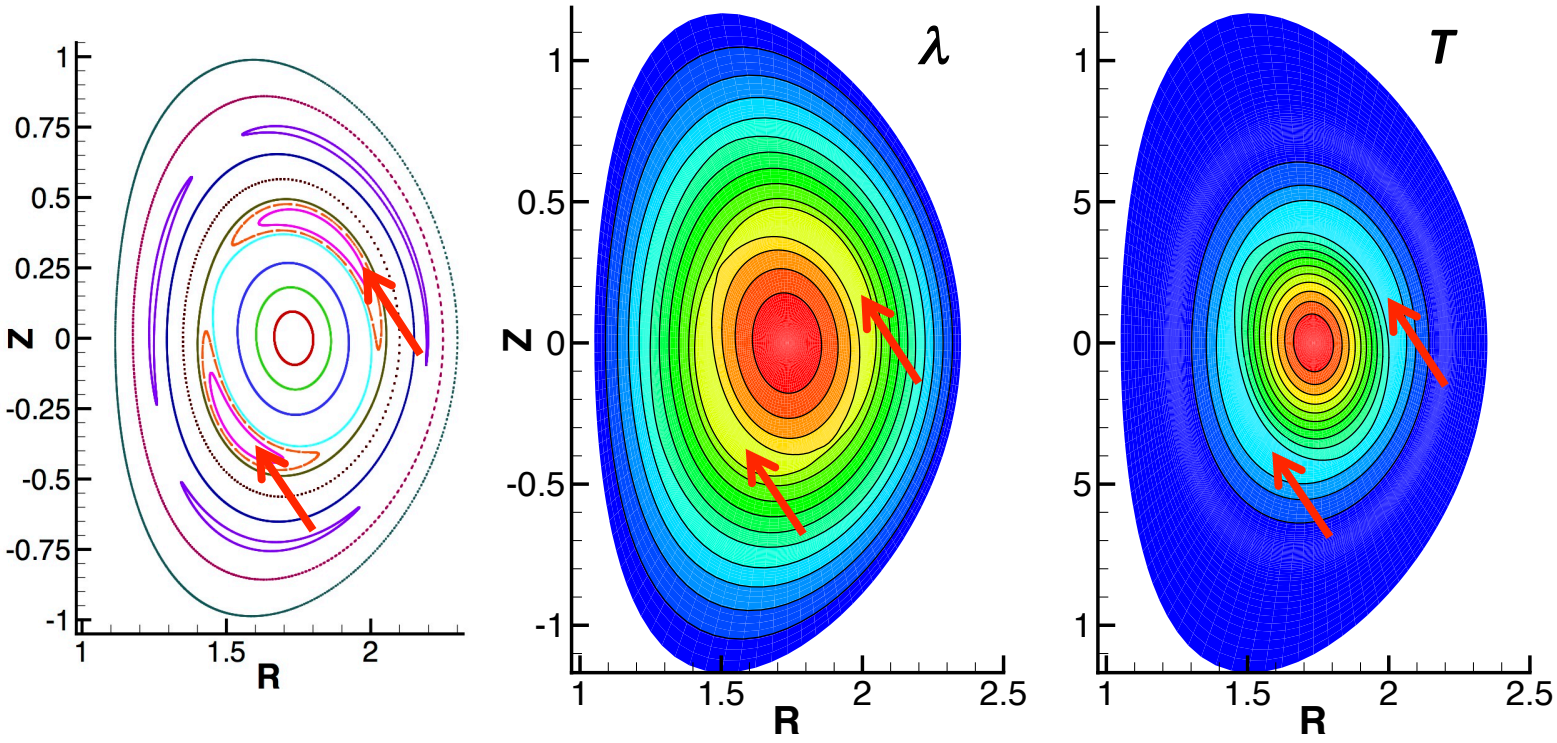

The island-evolution example saturates nonlinearly by making λ uniform along **B**, and strongly anisotropic $\underline{\boldsymbol{\kappa}}$ equilibrates *T* over the island.

Geometry is important for simulating macroscopic dynamics in experiments.

- Finite Fourier series for periodic coordinates is effective but geometrically limiting.
- Meshing two or all three coordinates enhances flexibility.

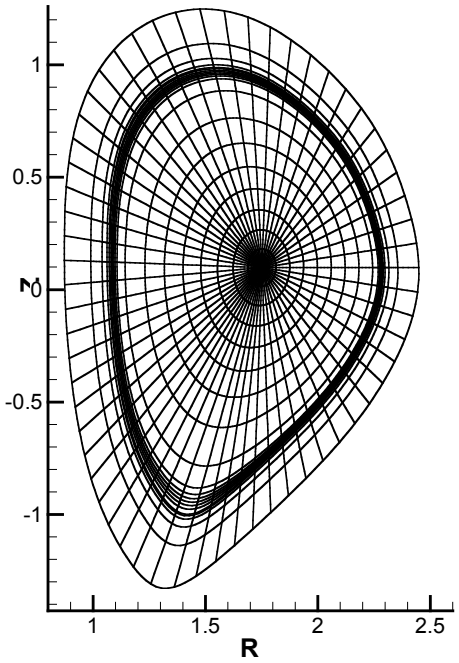

Packed mesh of curved 2D elements for modeling ELMS.

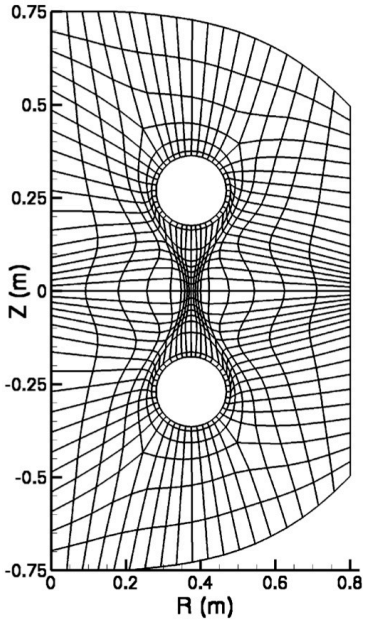

2D mesh for modeling MRX [Murphy, PoP **15**, 042313].

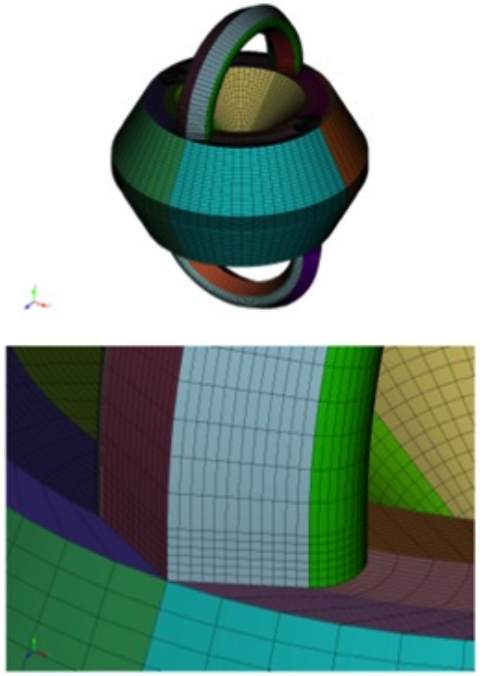

CAD-based 3D mesh for HIT-SI. [PSI-Center and CUBIT]

High-order elements and spectral representations are effective for anisotropic transport.

- A thermal-conduction test with analytical solution quantifies transport error.
- Results with high-order elements converge on extreme anisotropy without mesh alignment [Sovinec, et al., JCP **195**, 355].

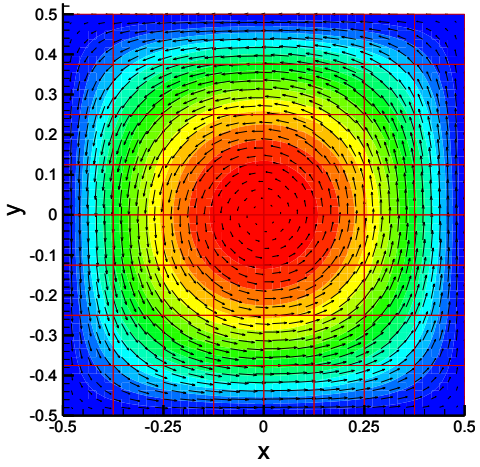

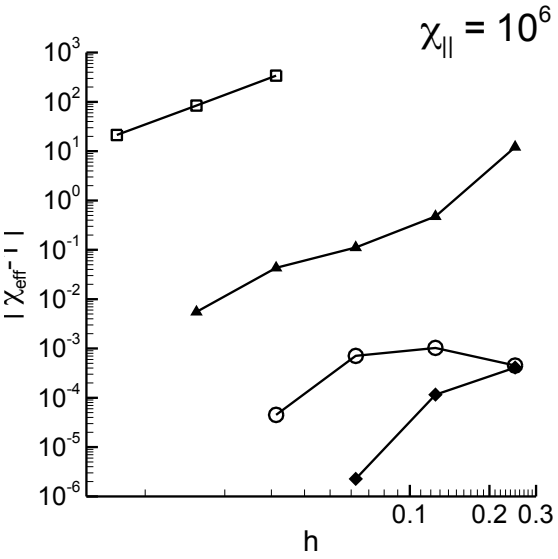

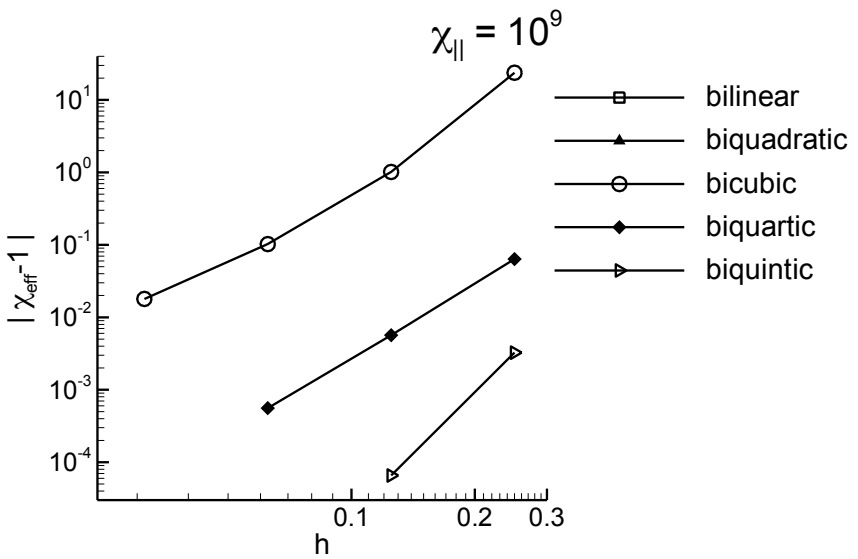

The test case has magnetic flux and $T \sim \cos(\pi x)\cos(\pi y)$.

Numerical error in perpendicular transport is quantified by the computed peak temperature as mesh size and polynomial bases are varied.

Element-based function spaces need to be suited for the system of equations.

- Dependent variables are expanded in polynomials within each element.
- Projections generate algebraic equations from the differential system.
- A 1D thermal-conduction example illustrates the process:

Solve $-\frac{d}{dx}\kappa(x)\frac{dT}{dx} = Q(x)$ in $0 \le x \le L$

subject to $T(0) = T_0\,, \quad -\kappa(L)\frac{\partial T}{\partial x} = q_L$

assuming $\kappa(x) > 0$.

- The formal solution $T(x) = T_0 + \int_0^x \frac{1}{\kappa(x'')}\left[\int_{x''}^L Q(x')\,dx' - q_L\right]dx''$ has continuous $T(x)$, but dT/dx is discontinuous at jumps in κ or point sources in Q.
- The suitable function space has C^0 continuity.

Finite-dimensional function spaces are defined by the choice of mesh and polynomials within each element.

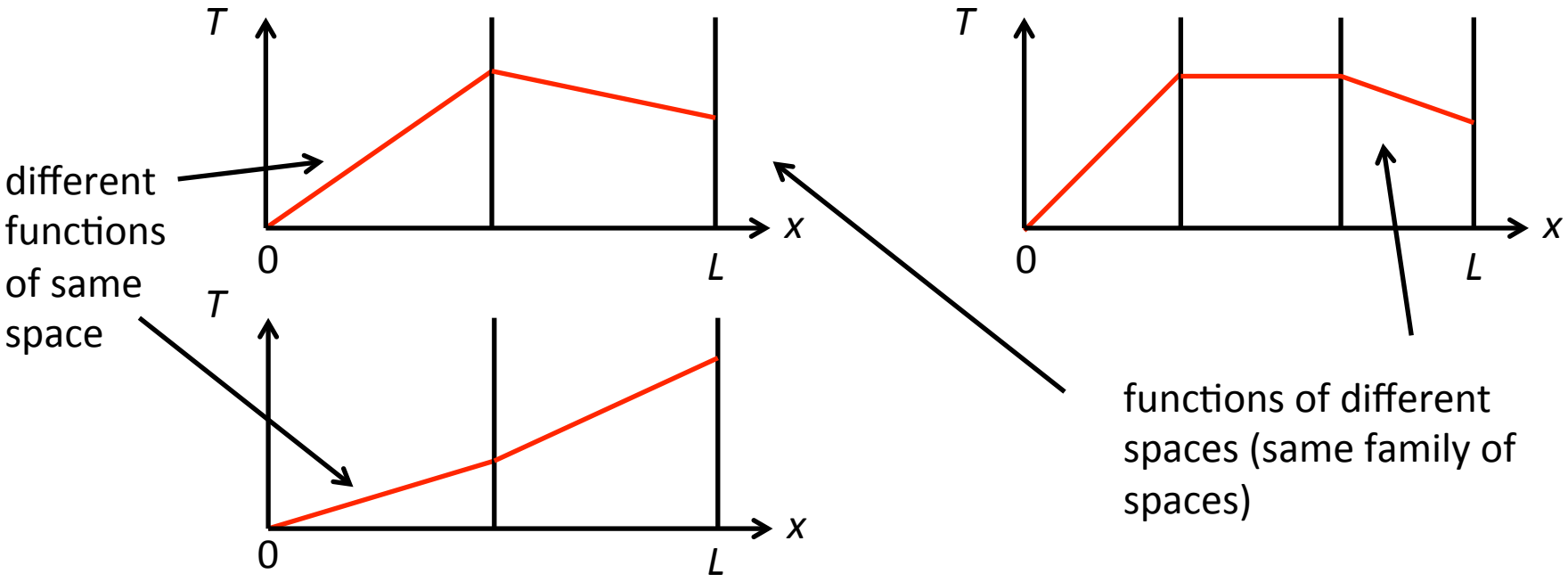

- The above sketches of linear elements illustrate finite-dimensional function spaces of C^0 continuity.
- $T(x)$ is a nodal expansion: $T^h(x) = \sum_i T_i \alpha_i(x)$

The weak form of an equation is used to select the best function from a given space.

- For a given mesh and basis, find $T^h(x) \in S^h$ such that

$$\int_0^L \left[\kappa \frac{d\Theta}{dx} \frac{dT^h}{dx} - \Theta Q \right] dx - q_L \Theta(L) = 0$$

for all $\Theta(x) \in S^h$.

- The integrals generate an algebraic system for the coefficients of T^h, symbolically expressed as

$$\underline{\underline{M}}\,\underline{T} = \underline{R}$$

- The first term in the integral is a mathematical energy that responds to all possible wiggles in the function space.

*See Strang and Fix, *An Analysis of the Finite Element Method* (1988).

There are spatial-representation challenges for MHD applications.

- Dissipative terms are second-order, so continuity requirements are similar to the conduction example.
  - However, dissipation is weak in high temperature plasma.

$$R_{cell} = \frac{\Delta x |\mathbf{V}|}{\nu} \begin{matrix} > \\ < \end{matrix} 1? \qquad S_{cell} = \frac{\Delta x v_A \mu_0}{\eta} \begin{matrix} > \\ < \end{matrix} 1?$$

- The ideal part of the primitive-field time-dependent equations have first-order spatial derivatives.
  - Galerkin projection does not respond to all wiggles.
- The $\nabla_{||}$ operator is singular for a helical distortion along its surface of resonance.
  - Free energy from bad curvature can excite mesh-scale oscillations.
- Satisfying the divergence constraint is not trivial for expansions of **B**.
- Unlike the simple example, identifying appropriate function-spaces for MHD and extended-MHD is not easy.

Consequences of a poor choice can be significant.

- Spectral pollution and numerical destabilization of physically stable interchange are well known concerns.
  - 2^{nd}-order ideal-MHD eigenvalue problems: [Gruber and Rappaz (1985); Degtyarev and Medvedev, CPC **43**, 29]
  - 1^{st}-order *t*-dependent: [Lütjens and Luciani, CPC **95**, 47; Sovinec, JCP **319**, 61]

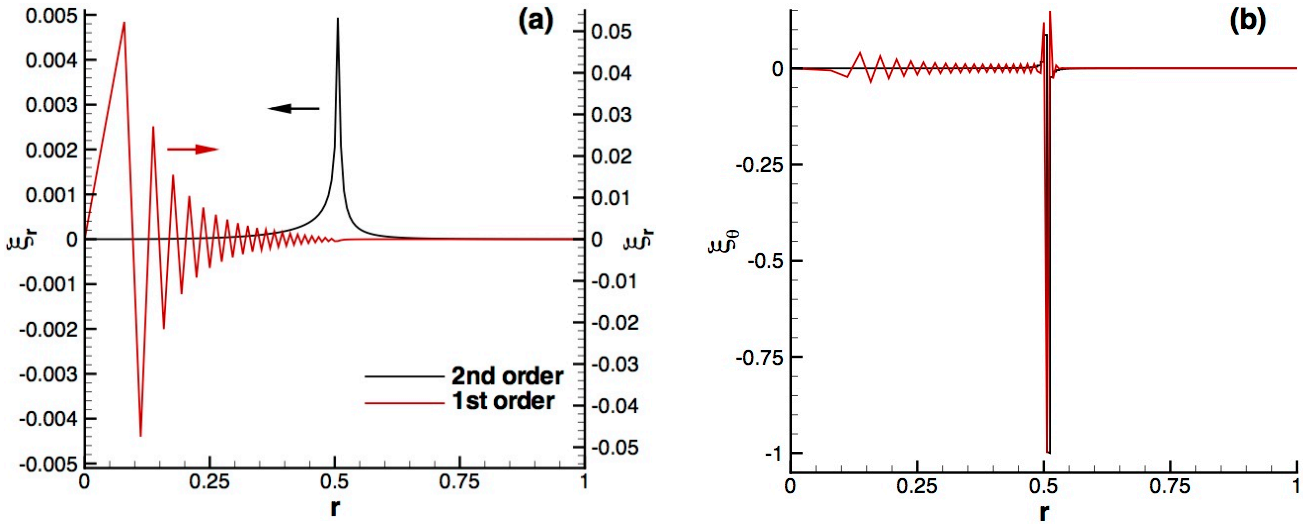

Components of a) radial and b) azimuthal displacement from 2^{nd}-order (black) and unstabilized 1^{st}-order (red) computations of marginally stable interchange.

- Physically representative behavior requires appropriate numerical responses to singular bending and compression at the limit of resolution.

Parallel computing: 3D domain decomposition is needed for large nonlinear problems.

- Domain decomposition is straightforward for element-based methods of generating algebraic systems.
- Codes using 3D elements, e.g. M3D-C1, decompose geometrically over all dimensions.
- Codes using finite Fourier series for one or two dimensions, e.g. NIMROD, decompose those dimensions by Fourier component.

✧ Solving the algebraic systems from implicit advances dominates parallel performance.

- CG and GMRES operations scale well, but they need preconditioning.
- Multigrid has optimal scaling but does not work well on all matrices.

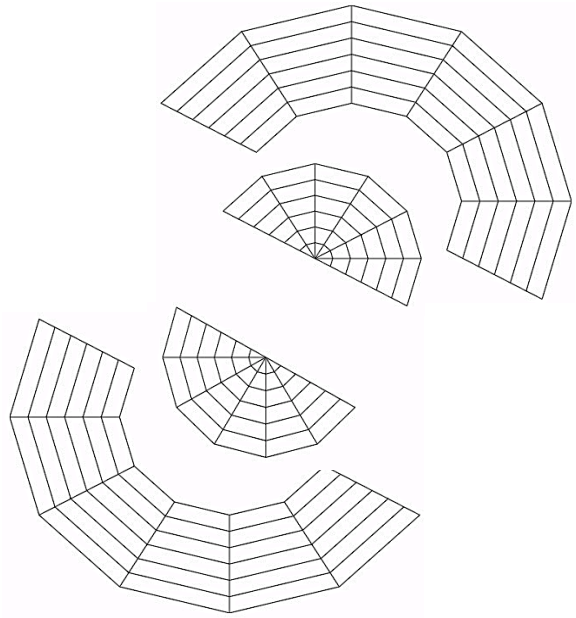

Mesh of 2D elements decomposed into blocks for parallel processing.

Distributed-memory parallelism with MPI communication has been the standard.

- The parallel performance of the preconditioning operations influences scaling and overall speed.

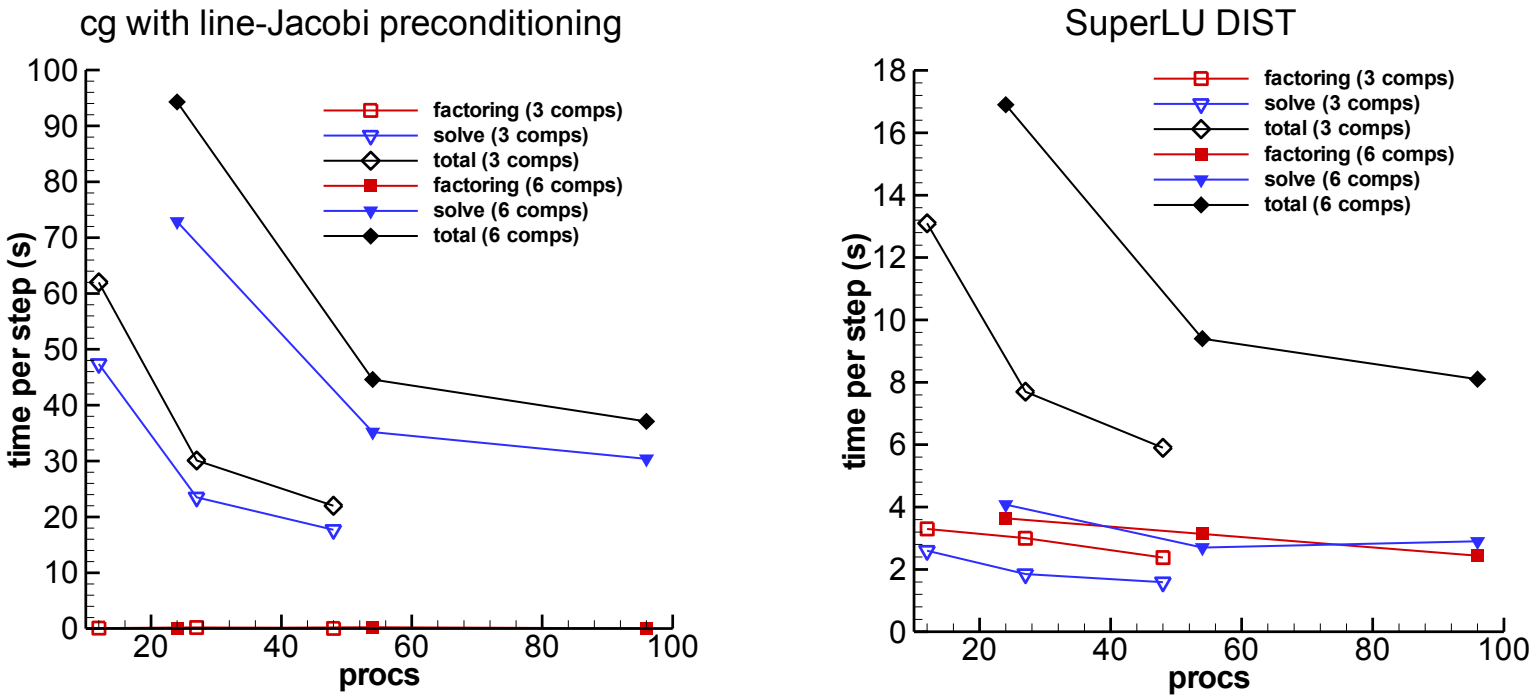

Strong-scaling tests on a small problem compare a less-effective preconditioner (left) with parallel sparse solves of diagonal blocks (right) [SuperLU: Li & Demmel ACM TMS **29**, 110].

Fusion MHD computing is gradually evolving from MPI to hybrid parallelization.

- Efficient use of on-node memory benefits from thread-based parallelism.
- Obtaining performance improvement requires directives, e.g. OpenMP.
- Jacob King, Tech-X, implemented and tested OpenMP in NIMROD.

Mira BlueGeneQ at ORNL has symmetric multi-processing (SMP) nodes.

- Each node has 16 cores.
- Hyper-threading *allows* over-subscription by up to 4.

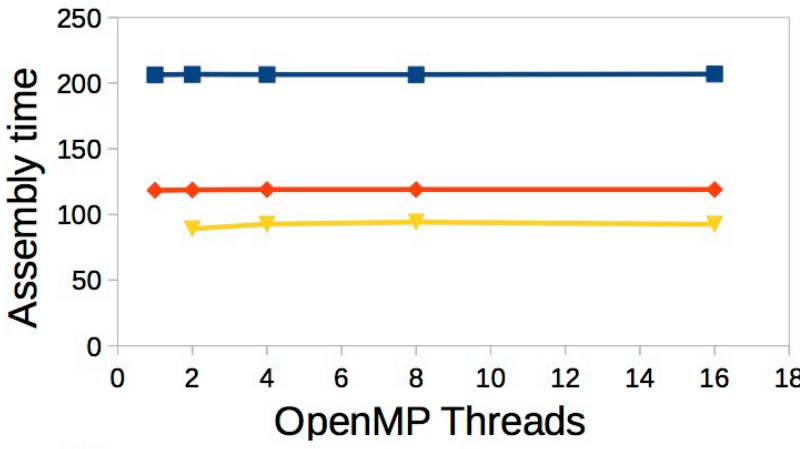

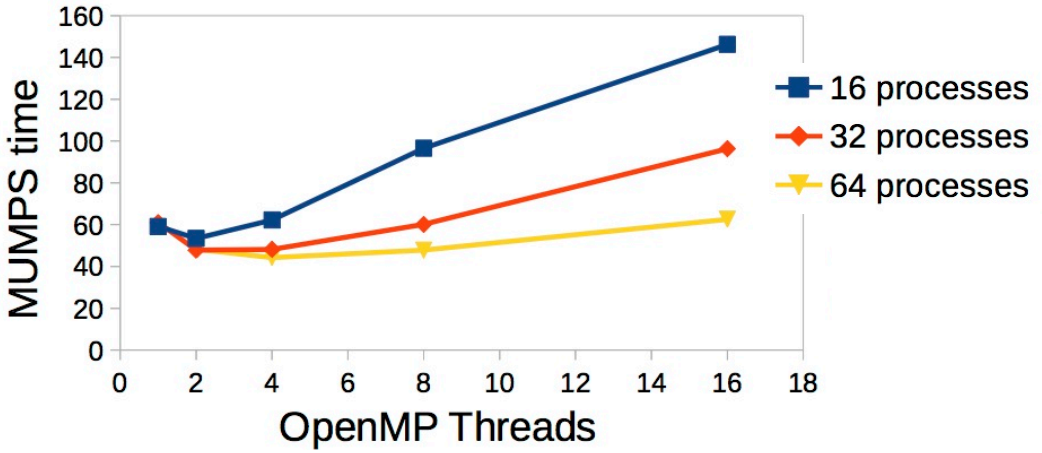

King's single-node tests with NIMROD + MUMPS 5.0.0 show:

- Exchanging MPI calls with OpenMP threads has little impact for FE "assembly."
- MUMPS 5.0.0 threading is better than MPI alone (1 vs. 2 threads).

Open Challenges and Outlook

- "Multi-physics" challenge: applications, such as tokamak disruption, requires more general physics modeling.
  - Electromagnetics interact with 3D external conductors.
  - Plasma-surface interaction affects plasma properties.
  - Neutral dynamics and radiation are important.
  - Runaway e^- form a significant new kinetic species.
- "Multi-scale" challenge: temporal and spatial scale separation remain primary applied-math considerations.
  - Ranges of scales in experiments increase with plasma performance.
  - Drift physics (even 2-fluid) introduces oscillations -> implicit $\Delta t > \omega^{-1}$??
  - SOLVERS, SOLVERS, SOLVERS
- Increasing hardware complexity is a challenge for implicit computation.
  - Frequent data movement is needed for implicit computation.
  - Solvers??

Addressing the challenges will need plasma theory, applied mathematics, and computer science.

- Code-coupling is often assumed to be the fastest approach to multi-physics simulation.
  - Implicit stepping may need outer iteration.
  - Coupling computations that use different representations needs more study.
- Hardware accelerators, e.g. GPUs, compounds data movement problems.
  - Computer-science development of algebraic solvers is needed.
  - Use for spatially local computations including v-space computation?
  - Revisit less-implicit methods?

❖ Cross-disciplinary teaming will continue to be the best approach to meeting the challenges of fusion MHD simulation.

Reference List

- Breslau, J, Ferraro, N, Jardin, S: Some properties of the M3D-C^1 form of the three-dimensional magnetohydrodynamics equations. Phys. Plasmas **16**, 092503 (2009)
- Caramana, EJ: Derivation of implicit difference schemes by the method of differential approximation. J. Comput. Phys. **96**, 484-493 (1991) Chacón, PoP **15**, 056102
- Degtyarev, LM, Medvedev, SYu: Methods for numerical simulation of ideal MHD stability of axisymmetric plasmas. Comput. Phys. Commun. **43**, 29-56 (1986) Gruber and Rappaz (1985)
- Hazeltine, RD, Meiss, JD: Plasma Confinement. Addison-Wesley, Redwood City (1992)
- Held, ED, Kruger, SE, Ji, J-Y, Belli, EA, Lyons, BC: Verification of continuum drift kinetic equation solvers in NIMROD. Phys. Plasmas **22**, 032511 (2015)
- Huysmans, GTA, Pamela, S, van der Plas, E, Ramet, P: Non-linear MHD simulations of edge localized modes (ELMs). Plasma Phys. Control. Fusion **51**, 124012 (2009) Kim, PoP **15**, 072507
- Kimura, K, Morrison, PJ: On energy conservation in extended magnetohydrodynamics. Phys. Plasmas **21**, 082101 (2014)
- Knoll, DA, Chacón, L, Margolin, LG, Mousseau, VA: On balanced approximations for time integration of multiple time scale systems. J. Comput. Phys. **185**, 583-611 (2003)
- Kruger, SE, Schnack, DD, Sovinec, CR: Dynamics of the major disruption of a DIII-D plasma. Phys. Plasmas **12**, 056113 (2005)
- Lerbinger, K, Luciani, JF: A new semi-implicit method for MHD computations. J. Comput. Phys. **97**, 444-459 (1991)
- Li, XS, Demmel, JW: SuperLU_DIST: a scalable distributed-memory sparse direct solver for unsymmetric linear systems, ACM Trans. Math. Software **29**, 110-140 (2003).
- Lütjens, H, Luciani, J-F: A class of basis functions for non-ideal magnetohydrodynamic computations. Comput. Phys. Commun. **95**, 47-57 (1996) Murphy, PoP **15**, 042313
- O'Bryan, JB, Sovinec, CR: Simulated flux-rope evolution during non-inductive startup in Pegasus. Plasma Phys. Control. Fusion **56**, 064005 (2014)

- Park, W, Monticello DA, Chu, TK: Sawtooth stabilization through island pressure enhancement. Phys. Fluids **30**, 285-288 (1987)
- Park, W, Parker, S, Biglari, H, Chance, M, Chen, L, Cheng, CZ, Hahm, TS, Lee, WW, Kulsrud, R, Monticello, D, Sugiyama, L, White, R: Three-dimensional hybrid gyrokinetic-magnetohydrodynamics simulation. Phys. Fluids B **4**, 2033-2037 (1992)
- Ramos, JJ: Finite-Larmor-radius kinetic theory of a magnetized plasma in the macroscopic flow reference frame. Phys. Plasmas **15**, 082106 (2008)
- Schnack, DD, Barnes, DC, Mikic, Z, Harned, DS, Caramana, EJ: Semi-implicit magnetohydrodynamic calculations. J. Comput. Phys. **70**, 330-354 (1987)
- Shokin, YI: The Method of Differential Approximation. Springer-Verlag, Berlin (1983)
- Sovinec, CR, Glasser, AH, Gianakon, TA, Barnes, DC, Nebel, RA, Kruger, SE, Schnack, DD, Plimpton, SJ, Tarditi, A, Chu, MS, the NIMROD Team: Nonlinear magnetohydrodynamics simulation using high-order finite elements. J. Comput. Phys. **195**, 355-386 (2004)
- Sovinec, CR, King, JR, the NIMROD Team: Analysis of a mixed semi-implicit/implicit algorithm for low-frequency two-fluid plasma modeling. J. Comput. Phys. **229**, 5803-5819 (2010)
- Sovinec, CR: Stabilization of numerical interchange in spectral-element magnetohydrodynamics. J. Comput. Phys. **319**, 61-78 (2016)
- Strang, G, Fix, GJ: An Analysis of the Finite Element Method. Wellesley-Cambridge Press, Wellesley, MA (1988)
- Strauss, HR: Nonlinear, three-dimensional magnetohydrodynamics of noncircular tokamaks. Phys. Fluids **18**, 134-140 (1976)

The ideal-MHD spectrum of a periodic cylinder illustrates different types of modes.

- There is a gap between the uniform-density "plasma" column $0 \le r \le 1$ and a conducting wall at $r = 1.5$.
- Spectra for $m = 1$, $k = -0.0445$ with varying levels of parabolic axial current density are evaluated for $\mu_0 J_{0_z} = J_0\left(1 - r^2\right)$ and $\beta(0)=2\%$.

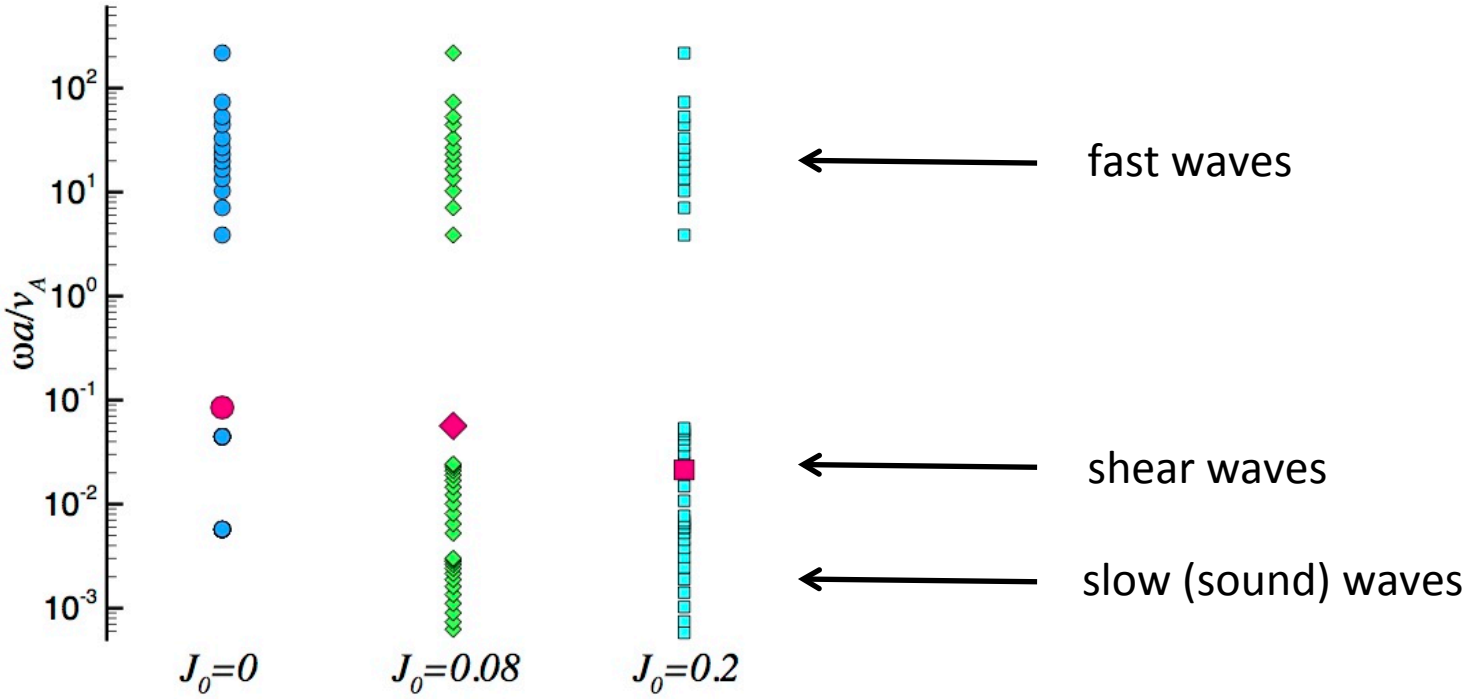

Magenta is an external mode that is unstable at $J_0 = 0.2$, where Im(ω) is shown.